基于视觉的激光深熔焊熔池检测及图像处理

杨家林[1]，　高进强[2]，　秦国梁[2]，　何建国[1]，　武传松[2]，　张　涛[2]

(1. 中国工程物理研究院 机械制造工艺研究所，绵阳　621900；
2. 山东大学 材料液固结构演变与加工教育部重点实验室，济南　250061)

杨家林

摘　要：针对不锈钢材料 Nd: YAG 固体激光深熔焊接，在充分分析熔池辐射光谱特征的基础上，并考虑同轴检测的技术特点，设计了熔池辐射光和 YAG 激光的传输与分离机构，优选了合适的半透半反镜片、窄带滤光片、中性减光片和变焦镜头等光路系统组件，成功构建了面向 Nd: YAG 激光深熔焊接的同轴视觉检测系统，获得了清晰的熔池区图像. 针对拍摄到的熔池区图像，设计了高斯函数滤波、边缘增强算子、边界跟踪算法等图像处理算法，确定了搜索起始点和搜索准则，较好地提取出熔池边缘，为下一步实现激光深熔焊的焊接质量在线实时监测与控制奠定了基础.

关键词：激光焊；熔池；边缘；图像处理算法

中图分类号：TG115.28　　**文献标识码**：A　　**文章编号**：0253－360X(2011)11－0021－04

0　序　　言

激光焊接被誉为 21 世纪最先进的焊接技术之一，在汽车、造船、航空航天、机械、电子仪表等行业得到了越来越广泛的应用. 为保证优良的焊接质量，必须对激光焊接质量进行控制. 激光深熔焊的熔池包含有丰富的焊接质量信息，直接决定焊缝成形和焊接质量.

视觉传感是目前最为先进、信息量最丰富的焊接过程检测方法，国内外对采用视觉传感进行激光焊接过程的监测进行了较为广泛的研究. Matsunawa 等人[1]采用旁轴式主动视觉传感技术拍摄熔池图像，但没有涉及熔深等参数与熔池几何参数的关系. 利用 CCD 摄像机从小孔正上方采集熔池及小孔的图像[2,3]，以图像灰度最大值作为特征参数，建立了图像灰度最大值与孔深的标定曲线，但图像灰度的最大值能否反映熔深还值得探讨. Beersiek[4]采用同轴视觉传感器拍摄了熔池图像，定性分析了熔池宽度与熔深的对应关系，但没有给出它们之间的定量关系. 秦国梁等人[5]针对碳钢 Nd: YAG 激光焊接，建立了同轴视觉传感检测系统，对熔池进行了检测. 为了建立熔池几何形状与焊接质量的关系，需要采用尽量多的熔池几何形状参数.

收稿日期：2010－09－16
基金项目：国家自然科学基金委员会－中国工程物理研究院联合基金资助项目(10776020)

采集清晰完整的熔池图像，并设计合适的图像处理算法是非常重要的. 文中在这方面进行了一些尝试，建立了激光深熔焊同轴检测系统，拍摄到了清晰的熔池区图像，设计了合适的图像处理算法，提取出了熔池的边缘，为实现激光深熔焊焊接质量的在线实时控制奠定了基础.

1　试验方法

试验采用 316L 不锈钢薄板，尺寸为 250 mm × 100 mm × 2 mm. 设备采用自主研制的 2 kW Nd: YAG 固体激光器，美国 Acton Research 公司生产的 SP556 平面影像光谱仪，美国 Priceton Instruments 公司生产的 TE/CCD-1100-PF 光谱探测器和和 ST-133CCD 光谱探测控制器. 试验中利用 YAG 激光，在不锈钢薄板上采用堆焊的方法，开展激光深熔焊熔池的同轴视觉检测系统构建和功能测试.

2　熔池辐射光谱特征分析

图 1 为激光深熔焊光谱测试系统，主要由 PC 机、平面影像光谱仪、CCD 光谱探测器及配套的光谱探测控制器组成.

图 2 和图 3 为激光功率(P)分别为 1.5 kW 和 2 kW 时测得的辐射光谱. 从光谱上看，600 ~ 650 nm 波段没有特征光谱，而该波段同轴辐射光相对较强. 同时考虑到该波段属于可见光波段，摄像机对

该波段比较敏感,因此选择 600 ~ 650 nm 作为熔池采集波段窗口.

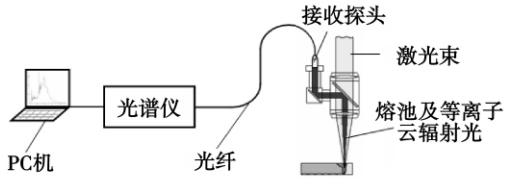

图 1 辐射光谱测试系统框图

Fig. 1 Schematic of spectrum analyzing system

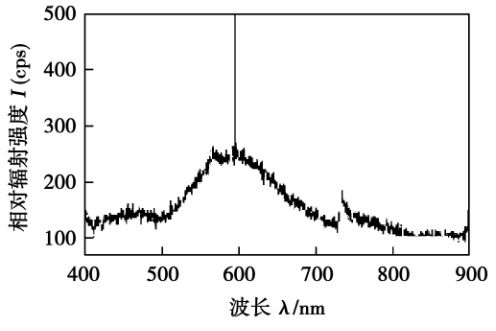

图 2 激光深熔焊同轴辐射光谱(P =1.5 kW)

Fig. 2 Co-axial radiation spectrum

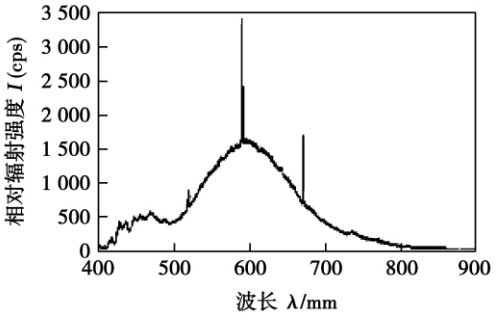

图 3 激光深熔焊同轴辐射光谱(P =2 kW)

Fig. 3 Co-axial radiation spectrum

3 同轴视觉传感检测系统构建

在激光光路中利用半透半反分光镜片,成功地将熔池的同轴成像信号从激光光路中分离出来,并根据熔池辐射光谱特征,构建了图 4 所示的同轴视觉检测系统,该系统主要由 PC 机、图像采集卡、摄像机、变焦镜头、内置半透半反分光镜片的激光输出镜头、窄带滤光片和中性减光片组成.

摄像机为 NTSC 制式的普通 CCD 彩色摄像机,分辨率为 456 × 608,采集频率为 25 帧/s. 激光输出镜头能够使YAG激光以很高的透过率通过,而来

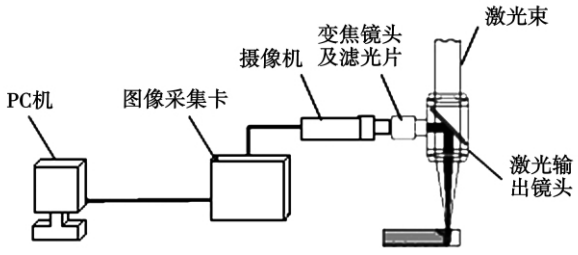

图 4 同轴视觉传感检测系统示意图

Fig. 4 Schematic of co-axial visual checking system

自熔池的可见光则被反射. 图 5 为在激光功率为 1.8 kW、焊接速度(v) 为 10 mm/s 条件下拍摄到的熔池图像,可见熔池区图像比较清晰.

图 5 熔池区图像

Fig. 5 Image of weld pool area

4 图像处理

4.1 图像转换

在试验系统中采集的图像是彩色图像,表色系为 RGB 表色系. 由于采用了中心波长处于 600 ~ 650 nm 范围内的窄带滤光片,该波长范围属于红光,因此在图像中,红基色对图像的贡献大. 为提高图像处理速度,文中只对红基色进行处理,将图像的红基色显示成灰度. 图 6 为将图 5 的红基色提取出

图 6 灰度图像及建立的坐标系

Fig. 6 Gray image and coordinate system

来后得到的灰度图像. 为了便于描述,建立图 6 所示坐标系 Oxy,Oij,其中 Oij 为离散坐标系.

4.2　图像滤波

采用高斯函数作为滤波器,高斯函数为

$$G(x,y,\sigma)=\frac{1}{2\pi\sigma^2}\exp\left(-\frac{1}{2\sigma^2}(x^2+y^2)\right) \quad (1)$$

式中:σ 为高斯函数参数,文中取 $\sigma=1$.

为了将式(1)用于数字图像,需将其离散化. 离散化后获得 5×5 模板. 将该模板与图像卷积,则可近似认为是采用高斯函数滤波器对图像进行滤波. 经高斯滤波后的图像如图 7 所示.

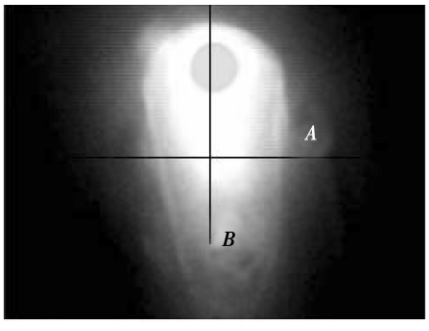

图 7　高斯滤波后的图像

Fig. 7　Gray image after gauss filtering

4.3　边缘增强

在图 7 中 A,B 两方向取图像的灰度值分布,如图 8 和图 9 中虚线所示. 从图中可以看出,熔池边缘属于斜坡渐变型边缘,需要对边缘进行增强,才能准确地提取出熔池的边缘.

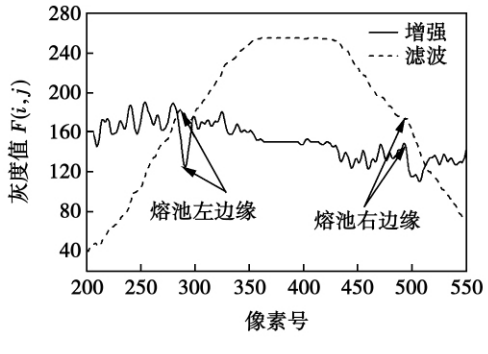

图 8　边缘锐化前后的 A 线灰度分布

Fig. 8　Gray along A line before and after enhancing

边缘增强算法为

$$F'(i,j)=k+F(i+3,j)+F(i+2,j)+F(i+1,j)-F(i-1,j)-F(i-2,j)-F(i-3,j) \quad (2)$$

式中:$F(i,j)$ 为像素点经高斯滤波后的灰度值;$F'(i,j)$ 为滤波增强后的灰度值,常数 k 取 150.

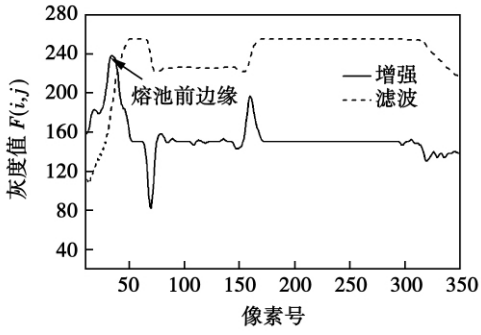

图 9　边缘锐化前后的 B 线灰度分布

Fig. 9　Gray along B line before and after enhancing

图 8 和图 9 中的实线是经过式(2)增强锐化后的 A,B 线灰度分布. 可以看出,经式(2)锐化后,搜索边缘转变为搜索锐化后曲线的极值点,熔池左边缘对应极小值点,右边缘对应极大值点.

4.4　熔池边缘提取

熔池边缘提取采用边界跟踪法. 边界跟踪效果的好坏主要取决于两个因素,即跟踪起始点的选取和跟踪准则的选取,这两个因素将直接影响到算法的难度和跟踪精度. 根据熔池特点,将熔池边缘提取分为两部分进行,即熔池头部搜索和熔池尾部搜索.

4.4.1　起始点的选取

从图 7 中可以看出,在熔池中部 A 线下方,熔池左右边缘基本上接近直线,利用熔池边缘的这一特点,可以比较准确地确定起始点. 在熔池中部选取 21 行,中心行用 j 表示. 在每一行,根据熔池边缘点特征,寻找左边缘点及右边缘点. 分别取 21 行左、右边缘点坐标值的平均值作为 j 行左、右边缘点坐标值 i_{ls},i_{rs}.

4.4.2　熔池尾部的搜索准则

熔池尾部的搜索准则如下. (1)左边缘必须是谷底,右边缘必须是波峰. (2)若存在多个谷底,寻找最低谷底,同时比较最低谷底与次低谷底之间灰度值差. 如果小于 5,则选取与上一搜索行的左边缘点最近的谷底作为候选左边缘点. 否则选择最低谷底作为候选左边缘点. (3)如果候选左边缘点横坐标与上一搜索行的左边缘点横坐标差值小于 3,则候选左边缘点记为左边缘点,否则此行左边缘点搜索失败,将上一搜索行左边缘点横坐标增加 1 作为本行左边缘点横坐标. (4)若存在多个波峰,寻找最高波峰,同时比较最高波峰与次高波峰之间灰度差. 如果小于 5,则选取与上一搜索行的右左边缘点最近的波峰作为候选右边缘点. 否则选择最高波峰作为候选右边缘点. (5)如果候选右边缘点横坐标与

上一搜索行右边缘点的横坐标差值小于 3，则候选右边缘点记为右边缘点，否则此行右边缘点搜索失败，将上一搜索行的右边缘点横坐标减 1 作为本行右边缘点横坐标.

4.4.3 熔池头部的搜索准则

熔池头部的搜索准则：(1) 头部边缘必须是波峰. (2) 若存在多个波峰，寻找最高波峰，同时比较最高波峰与次高波峰之间的差值. 如果小于 5，则选取与上一搜索列的头部左边缘点最近的波峰作为头部边缘点. 否则选择最高波峰作为本列头部边缘点.

为了减小计算量和准确性，对搜索范围做了限定，若刚确定的右列头部边缘点纵坐标用 j_r 表示，则本列搜索范围定为 $[j_r-30, j_r+30]$. 考虑到边缘的连续性，对搜索后的边缘进行了均值平滑处理. 搜索得到熔池边缘如图 10 所示，可以看出，设计的图像处理算法能较好地提取出熔池边缘.

图 10 搜索得到的熔池边缘

Fig. 10 Edge of laser weld pool after searching

5 结 论

(1) 构建了同轴视觉检测系统，获得了完整的激光焊接熔池二维图像.

(2) 分析了不锈钢激光熔池图像的特点，设计了高斯滤波算法、边缘增强算法，边界跟踪算法，确定了熔池边缘搜索起始点和搜索准则，较好地提取出了熔池边缘.

参考文献:

[1] Matsunawa A, Seto N, Kin J D, *et al*. Dynamics of keyhole and molten pool in high power CO_2 laser welding [C] // Proceedings of SPIE-The International Society for Optical Engineering, Osaka, Japan, 2000: 34 - 45.

[2] Abels P, Kaierle S, Kratzsch C. Universal coaxial process control system for laser material processing [C] // Proceedings of the 18th International Conference on Applications of Lasers and Electro-Optics, San Diego, California, USA, 1999: 99 - 108.

[3] Kratzsch C, Abels P, Kaierle S. Coaxial process control during laser beam welding of tailored blanks [C] // Proceedings of SPIE-The International Society for Optical Engineering, Osaka, Japan, 2000: 472 ~ 782.

[4] Beersiek J. A CMOS camera as a tool for process analysis not only for laser beam welding [C] // Proceedings of the 20th International Conference on Applications of Lasers and Electro - Optics, Jacksonville, Florida, USA, 2001: 206 - 215.

[5] 秦国梁，王旭友，林尚扬. 大功率 Nd: YAG 激光焊接过程同轴视觉传感 [J]. 机械工程学报，2004，40(7)：184 - 189.
Qin Guoliang, Wang Xuyou, Lin Shangyang. Coaxial visual sensing technology in Nd: YAG laser welding with high power [J]. Chinese Journal of Mechanical Engineering, 2004, 40(7): 184 - 189.

作者简介: 杨家林，男，1971 年出生，硕士，高级工程师. 主要从事高能束加工和激光快速制造技术方面的科研工作. 发表论文 60 余篇. Email: myyangjialin@ yahoo. com. cn

通讯作者: 高进强，男，教授. Email: jqg@ sdu. edu. cn

clad against 304 stainless steel under no-lubrication condition were evaluated on an UMT-2MT tester. Results showed that the sprayed Cu14Al4.5FeNiCe clad combined firmly to the 45 carbon steel substrate in a metallurgy way with a surface hardness of HB 320. The clad was composed of ($\alpha + \gamma_2$), β' and K phases, in which K phase was dispersed into the matrix of ($\alpha + \gamma_2$) and β'. The clad presented a good anti-lubrication character with friction coefficient of 0.105 under the load of 40N (5.7 MPa). Friction coefficient of the Cu14Al4.5FeNiCe clad against 304 stainless steel increased slightly with load increasing. The clad exhibited a high wear-resistance to 304 stainless steel, wear rate of the clad increased smoothly with load.

Key words: sprayed clad; microstructure; wear mechanism; tribology property

Vision-based checking and image processing for melt pool of laser deep penetration welding YANG Jialin[1], GAO Jinqiang[2], QIN Guoliang[2], HE Jianguo[1], WU Chuansong[2], ZHANG Tao[2] (1. Institute of Machinery Manufacturing Technology, China Academy of Engineering Physics, Mianyang 621900, China; 2. Key Laboratory for Liquid-Solid Structural Evolution & Processing of Materials Ministry of Education, Shandong University, Jinan 250061, China). p 21 - 24

Abstract: On the basis of analyzing the infrared spectrum characteristics of weld pool by Nd: YAG laser, the co-axial visual monitoring system for Nd: YAG laser deep penetration welding of stainless steel was constructed successfully, by designing the transmitting and separating structure for weld pool radiation and YAG laser, and then optimizing the suitable light components, such as half penetrating and half reflecting lens, narrow band pass filter, neutral weakener, variable-focus lens and so on, according to the requirements of co-axial monitoring. By means of the developed monitoring system, the clear images of weld pool were attained. In allusion to the recorded image of weld pool, gauss filter, edge enhancing function and algorithm for edge tracking were developed, by which the starting point and rules for edge tracking were put forward. Consequently, the edge of Nd: YAG laser welding pool was extracted from CCD images, which would be helpful to the on-line monitoring and controlling of laser deep penetration welding for better welding quality in future.

Key words: laser welding; weld pool; edge; image processing & algorithm

Curved convex face residual stress measurement by ultrasonic method MA Ziqi[1], LIU Xuesong[1], ZHANG Shiping[2], CHENG Yi[3], FANG Hongyuan[1] (1. State Key Laboratory of Advanced Welding and Joining, Harbin Institute of Technology, Harbin 150001, China; 2. School of Electrical Engineering and Automation, Harbin Institute of Technology, Harbin 150001, China; 3. Harbin Welding Training Institute, Harbin 150046, China). p 25 - 28

Abstract: An ultrasonic residual stress measurement system was developed to detect residual stress on curved convex face with one-emit-one-receive transducer. Compared with the results of laser holography orifice method, the distribute section of tensile stress and compression stress are similar, both max tensile and compression stress of ultrasonic method are much lower than that of laser holography orifice method, and stress distribution line is more gently as well. According to the couple condition of transducer and analysis of the nominal acoustic coefficient, the results of ultrasonic residual stress measurement on curved convex face should be corrected with radius of curvature in order to get precision residual stress.

Key words: ultrasonic method; welding residual stress; curved face; coupling state; acoustic-elastic constant

CO_2 arc welding detection based on theory of weak periodic and multi-channel signals with normal repetition rate GAO Liwen[1,2], XUE Jiaxiang[1], ZHANG Wen[1], LIN Fang[1], CHEN Xiaofeng[1] (1. School of Mechanical and Automotive Engineering, South China University of Technology, Guangzhou 510640, China; 2. College of Information Technology, Guangzhou University of Chinese Medicine, Guangzhou 510006, China). p 29 - 32

Abstract: Aiming at the automatic detection on arc welding stability, this paper proposed the theory of weak periodic and multi-channel signals with normal repetition rate. Through a scientific mathematical deduction, an equation has been put forward, which can sufficiently demonstrate the dynamic characteristics of the repetition rate of periodic signal. To overcome the problems brought in by scattered signals during actual sampling, this paper has introduced a method by subdividing a signal point into countless micro points which normally distribute in a multi-dimensional signal space. Therefore, an important parameter of the equation, the generalized actual area could be reasonably calculated, through which the whole equation could be accurately solved. 104 times of arc welding electric signals were conducted as samples. Based on the probabilistic neural network (PNN), the samples has been trained and tested, which show that the dynamic characteristics drawn through the above-mentioned theory are closely related to the stability of CO_2 arc welding, and thereby the automatic detection can be realized.

Key words: CO_2 arc welding, stability, multi-channel signal; normal distribution

A multi-scale fractal image segmentation method for arc welding pool GAO Fei[1], WANG Kehong[1], LIANG Yongshun[2], ZHAN Lanlan[1], ZHANG Yan[1] (1. School of Materials Science and Engineering, Nanjing University of Science & Technology, Nanjing 210094, China; 2. School of Sciences, Nanjing University of Science & Technology, Nanjing 210094, China). p 33 - 36

Abstract: An individual section of the arc welding pool image has a close relationship with the ultimate weld seam formation. An analysis on the fractal dimension and multi-scale fractal feature of the slag and the weld pool part is performed, and the definitions of graphical fractal dimension and multi-scale fractal feature are also elaborated. An image segmentation method using both single fractal dimension algorithm and multi-scale fractal feature-based algorithm is introduced, which has been applied in the processing of arc welding images. Experiments show that the